Eur. Phys. J. B **25**, 177–189 (2002)
DOI: 10.1140/epjb/e20020020

THE EUROPEAN PHYSICAL JOURNAL B
EDP Sciences

Modeling of the current lines in discontinuous metal/insulator multilayers

F. Ernult[1,a], L. Giacomoni[1], A. Marty[1], B. Dieny[1], A. Vedyayev[2], and N. Ryzhanova[2]

[1] CEA/Grenoble, Département de Recherche Fondamentale sur la Matière Condensée, SP2M/NM, 38054 Grenoble Cedex 9, France
[2] Moscow Lomonosov University, Department of Physics, Moscow, 119699, Russian Federation

Received 9 October 2001

Abstract. Discontinuous magnetic metal/insulator multilayers are formed of equally spaced layers of magnetic particles embedded in an insulating matrix. Their electronic transport properties result from spin-polarized electron tunneling and Coulomb blockade effect. The current-in-plane (CIP) and current-perpendicular-to plane (CPP) resistances change by several orders of magnitude when the thicknesses of the metallic or insulating layers are varied. Calculations of the shape of the current lines in these multilayers are presented. It is shown that pure CIP or CPP transport occur in these systems only when the CIP or CPP resistances are very different in magnitude. If the two resistances are of the same order of magnitude, then the measured transport properties in both geometries are a combination of CIP and CPP transport.

PACS. 73.40.Rw Metal-insulator-metal structures – 73.40.Gk Tunneling – 73.61.-r Electrical properties of specific thin films

1 Introduction

Discontinuous magnetic metal/insulator multilayers constitute a new class of metal/insulator systems [1,2], intermediate between tunnel junctions [3] and CERMET films [4]. They are grown as metallic multilayers by sequential deposition of metallic and insulating layers. For certain couples of metal/insulating materials, the metal does not wet on the insulating layers and coalesce in the form of disjointed metallic patches. The resulting structure consists of layers of magnetic metallic particles embedded in an insulating matrix. Examples of multilayers having such a structure and which exhibit magnetoresistance effects associated with spin-polarized tunneling are (Co/SiO_2) [1], ($CoFe/HfO_2$) [2], (Co/ZrO_2). As in Cermets, their transport properties result from a combination of spin-polarized electron tunneling through the insulating barriers separating neighboring metallic particles and of Coulomb blockade effect [5]. In contrast to Cermets and because of their particular structure, these mulilayers have very anisotropic transport properties.

In the following of the paper, we consider a discontinuous metal/insulator multilayer comprising n metallic layers sandwiched between $(n + 1)$ oxide layers. We suppose that two metallic electrodes, a few millimeters apart, have been deposited on top of the structure for CIP transport measurement. For simplicity, we suppose here that two-point measurements are performed. We define R_{CIP} as the CIP resistance measured between these two electrodes. Similarly, we assume that two metallic electrodes have been placed, one at the bottom, the other at the top of the structure for CPP-transport measurements. We define R_{CPP} as the resistance measured between these two electrodes. Several transport regimes can be qualitatively distinguished depending on the relative values of R_{CIP} and R_{CPP} (see Fig. 1):

For the CIP measurements (Fig. 1a):

1. If $R_{\mathrm{CIP}} \ll R_{\mathrm{CPP}}$, the electrons only flow in the top metallic plane of particles. The measured CIP resistance corresponds then to the resistance of the first plane of metallic particles only.
2. If $R_{\mathrm{CIP}} \gg R_{\mathrm{CPP}}$, just below the electrodes, the electrons spread over all metallic layers and then flow in parallel within each metallic planes. In this limit, the current is equal in all planes. The measured resistance corresponds then to the resistance of all the metallic layers connected in parallel.
3. If $R_{\mathrm{CIP}} \approx R_{\mathrm{CPP}}$, the situation is intermediate between the two previous cases. The electrons flow in the various planes of particles but with unequal intensities.

The two first cases correspond to pure CIP regimes whereas the third one is a combination of CIP and CPP characteristics.

[a] e-mail: fernult@cea.fr

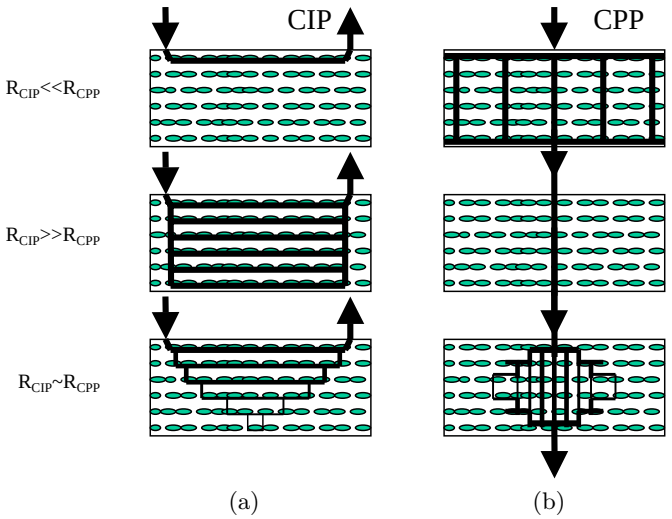

Fig. 1. Qualitative illustration of the three possible regimes of CIP transport (left (a)) and CPP transport (right (b)) in discontinuous multilayers.

Similarly, in CPP geometry, the same three cases lead to three different regimes (Fig. 1b):

1. If $R_{\mathrm{CIP}} \ll R_{\mathrm{CPP}}$, in the first metallic layers, the electrons spread over the whole area of the sample to minimize the perpendicular resistance as much as possible and then flow in parallel in the perpendicular direction across the thickness of the structure, the layers are nearly equipotentials. The whole area of the sample participates here to the CPP conduction.
2. If $R_{\mathrm{CIP}} \gg R_{\mathrm{CPP}}$, the electrons do not spread aside of the metallic electrodes. They just flow in parallel in the direction perpendicular to the interfaces below the electrodes. In that case, the area of the sample that is active for the perpendicular conduction is just the area of the CPP metallic electrodes.
3. If $R_{\mathrm{CIP}} \approx R_{\mathrm{CPP}}$, a combination of the two previous cases occurs. As they flow towards the median plane of the structure, the electrons propagate also within the metallic planes. Below the median plane, they concentrate again towards the bottom metallic electrode (see Fig. 1b).

The two first cases correspond to pure CPP transport situations whereas the third one is a combination of CIP and CPP transport characteristics.

From an experimental point of view, the in-plane resistance can be changed over several orders of magnitude by varying the nominal thickness of the metallic layers. This is illustrated in Figure 2 in the case of $(\mathrm{Co\ t(nm)/ZrO_2\ 30\,nm})_{20}$. The CIP resistance was measured at 300 K and 97 K with a four-point probe. These curves indicate the presence of a percolation threshold in each metallic plane occuring for a Co thickness of the order of 1.3 nm. Below this thickness, the CIP resistance increases dramatically and the resistance decreases with temperature, as in Cermets, due to Coulomb blockade effects. In contrast, above 1.3 nm, the resistance increases with temperature as usual in metallic films because of

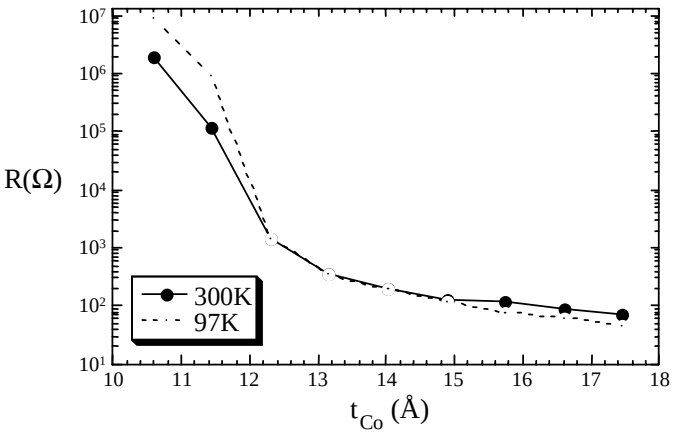

Fig. 2. In-plane resistance of a series of multilayers of the composition Co t_{Co}/ZrO_2 3.5 nm.

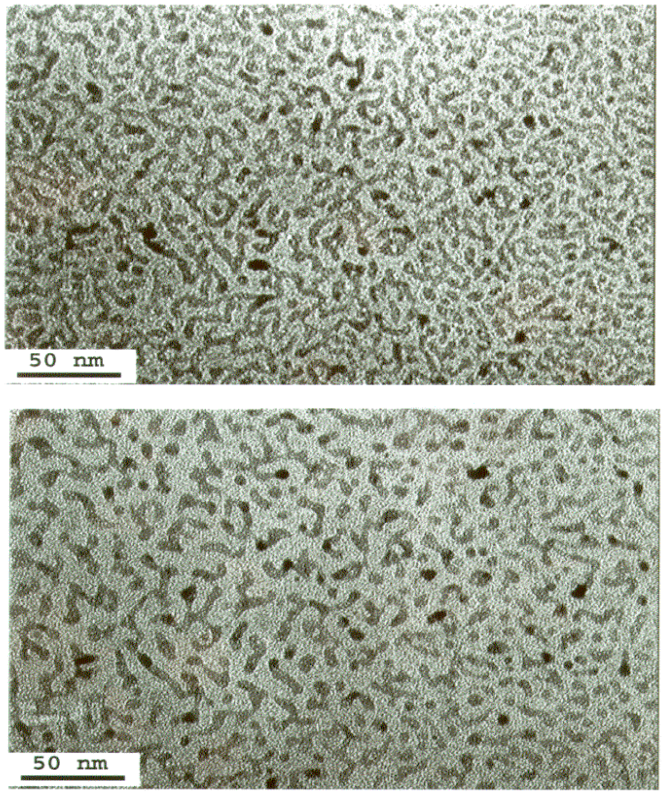

Fig. 3. Plane view observations by transmission electron microscopy of a single layer of Co particles, of nominal thickness 2 nm, inserted between 20 nm thick SiO_2 layers. Top: as-deposited sample; Bottom: after annealing at 300 °C for 1 hour.

phonon and magnon scattering. The CIP resistance varies also significantly upon sample annealing. Anneals favor the coalescence of the metallic patches into more compact and rounder particles. This is illustrated in Figure 3 which shows TEM plane views of single layers of Co inserted between SiO_2 layers before and after a 300 °C annealing for one hour. The coalescence of the Co particles is very clear in Figure 3.

Similarly the CPP resistance can be tuned over several orders of magnitude by changing the thickness of the insulating layer. The resistance of a tunnel barrier indeed increases exponentially with its thickness.

The CIP transport properties are usually investigated using a four-point probe geometry. Typical spacing between the voltage electrodes is a few millimeters. The CPP transport properties can be measured by depositing metallic crossed stripes at the bottom and top of the multilayered structure. These electrodes are used for the current and voltage contacts. The spacing between the electrodes across the thickness of the multilayered structure is typically a hundred nanometers. There are therefore 4 or 5 orders of magnitude between the probe spacing in CIP and CPP geometries. In metallic multilayers for which the CIP and CPP resistivities are of the same order of magnitude, this leads to an extremely low CPP resistance compared to the CIP resistance [6]. However, in the present multilayers, the spacing between two particles belonging to the same metallic plane is usually much smaller (less or of the order of a nanometer) than the spacing between two particles belonging to adjacent planes (2 or 3 nanometers). This results in an average CIP conductivity within the metallic plane higher by several orders of magnitude than the average CPP conductivity. Consequently, the much larger spacing between the voltage probe in the CIP geometry compared to the CPP geometry can be compensated by the much higher CIP than CPP conductivity resulting in the possibility of obtaining CIP and CPP resistances of comparable orders of magnitude. We emphasize that this is a rather unique feature of these systems. In metallic multilayers, the CPP resistance is always much lower than the CIP resistance. In tunnel junctions, the opposite is true.

Qualitatively, the mixing between the CIP and CPP regimes when R_{CIP} and R_{CPP} are of the same order of magnitude shows up very clearly in the measurements of the CIP I(V) characteristics. Indeed, in the pure CIP regime, the I(V) characteristics should always be linear. There are indeed typically 10^6 metallic particles and tunnel junctions connected in series between the CIP electrodes. The voltage across each of these junctions is therefore a tiny fraction of the total voltage so that all of the junctions operate in the linear part of their tunnel I(V) characteristics. The situation is different in CPP geometry. Indeed, in that case, the number of particles and tunnel junctions acting in series between the CPP electrodes is of the order of the number of repeats in the multilayered structure (typically of the order of 10). The voltage across each tunnel junction in the CPP geometry is therefore a significant fraction of the total CPP voltage. If voltages up to a few volts are applied, deviation from linear I(V) characteristics can be observed.

In the limits $R_{\mathrm{CIP}} \gg R_{\mathrm{CPP}}$ or $R_{\mathrm{CIP}} \ll R_{\mathrm{CPP}}$, pure CIP or CPP regimes occur and the CIP characteristics are linear. In contrast, if $R_{\mathrm{CIP}} \approx R_{\mathrm{CPP}}$, a mixing between CIP and CPP regimes occur so that non-linearities appear in the CIP I(V) characteristics. This is illustrated in Figure 4 which shows CIP and CPP I(V) characteristics

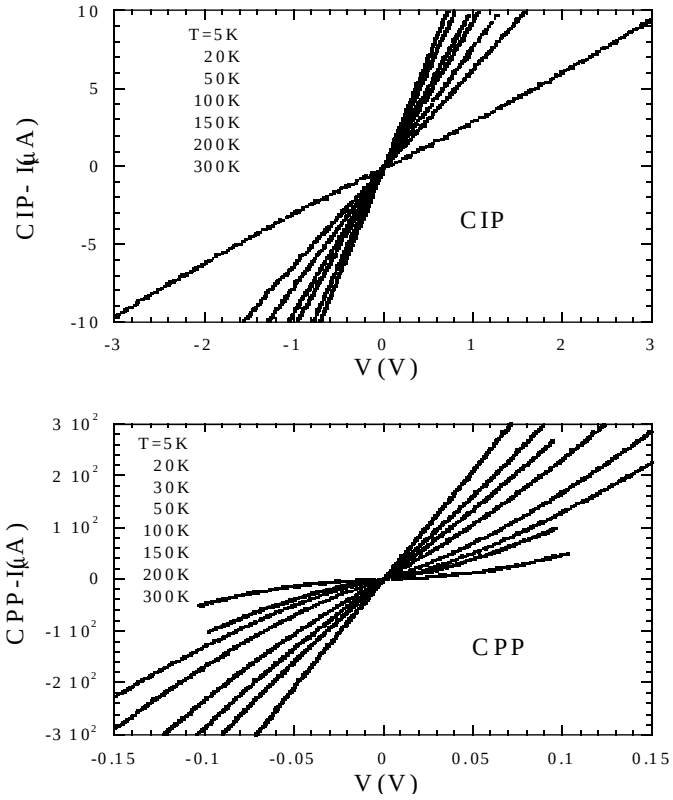

Fig. 4. CIP and CPP I(V) characteristics measured on a discontinuous multilayer of the composition $(\mathrm{Co}, 2\ \mathrm{nm}/\mathrm{SiO_2}, 3\ \mathrm{nm})_{16}$.

measured in discontinuous multilayers of the composition $(\mathrm{Co}\ 2\,\mathrm{nm}/\mathrm{SiO_2}\ 3\,\mathrm{nm})_{16}$ at various temperatures. In this multilayer, the CIP resistance decreases from 300 kΩ at 5 K to 160 kΩ at 300 K whereas the CPP resistance decreases from 30 kΩ at 5 K to 230 Ω at 300 K. As in Cermets, this increase of resistance at decreasing temperature is due to Coulomb blockade effects. The larger increase observed in CPP than in CIP implies that in CIP, because of the in-plane distribution of metallic particles, the current can flow dominantly through relatively large particles for which the Coulomb blockade is not very effective in the range of temperature investigated. In contrast, in CPP transport, the current can be forced to flow through smaller particles for which Coulomb blockade effects are observable above 5 K. As a result, $R_{\mathrm{CIP}}/R_{\mathrm{CPP}}$ is of the order of 10 at 4 K and of the order of 1000 at 300 K. Consequently, the I(V) characteristics are linear at 300 K whereas a slight curvature is observed on the I(V) curves at 5 K (see Fig. 4).

As explained previously, the metal/insulator granular systems give rise to complex transport phenomena such as Coulomb blockade effect. It is therefore difficult to simulate the transport properties of such systems. Many papers have studied the Coulomb blockade effects between magnetic particles [7,8], but the results obtained are difficult to apply to an assembly of particles (in a macroscopic sample counting about 10^6 particles). However, it may be

possible thanks to simpler models to determine the shape of the current lines for different values of the ratio $\frac{R_{\mathrm{CIP}}}{R_{\mathrm{CPP}}}$, and then to give a qualitative explanation to the curvature of the I(V) CIP characteristics. In order to describe the shape of the current lines in such macroscopic systems, we propose two different techniques: the first one consists in modeling the sample by a continuous anisotropic medium. In this model, the discrete effects are not taken into account, but it is possible to obtain analytical expressions of the current and of the resistance of the sample.

The second model takes into account these discrete effects by modeling the sample with an anisotropic network of resistances corresponding to the tunnel junctions between successive metallic clusters.

2 Conformal transformations

In the first part of the paper, the system is modeled by a continuous anisotropic medium. The shape of the current lines is then derived by using conformal transformations[1] in the complex plane (x, y). It immediately appears, that discrete effects (such as the finite number of particles) are not taken into account by this method. Furthermore, the calculations will be made in the linear regime in which the current is proportional to the potential. Consequently, the curvature of the I(V) characteristics cannot be modeled.

The conformal transformation calculation is a 2D calculation, the system is then invariant by translation along the z-axis. For the details of the calculations, see Appendix A.

2.1 Semi-infinite sample

First of all, we will study a semi-infinite sample (*i.e.* with a given thickness, but with an infinite length, then corresponding to an infinite stripe in the (X, Y) plane), which is is generally the case of macroscopic multilayers where $l > 100h$ (with l the length of the sample, and h its height).

Figure 5 shows the shape of the current lines in the CPP configuration, while Figure 6 shows their shape in the CIP configuration. One first notice that the boundary conditions are respected since the equipotential lines are perpendicular to the edges of the sample, *i.e.* no current flows through these edges. Furthermore, it immediately appears that the results of the calculation correspond to the qualitative picture shown in Figure 1, thus indicating a mixing between the CIP and CPP propagation modes depending on the value of the ratio $\epsilon = \frac{\sigma_y}{\sigma_x}$.

Figure 7 shows the conductance of the sample as a function of its thickness in CIP mode. It clearly evidences a non-linearity of the conductance *versus* the thickness of the film due to a change in the shape of the current lines as the thickness of the film varies. This graph also shows that this non-linearity is more or less pronounced depending on

[1] for more details about this technique, see [9].

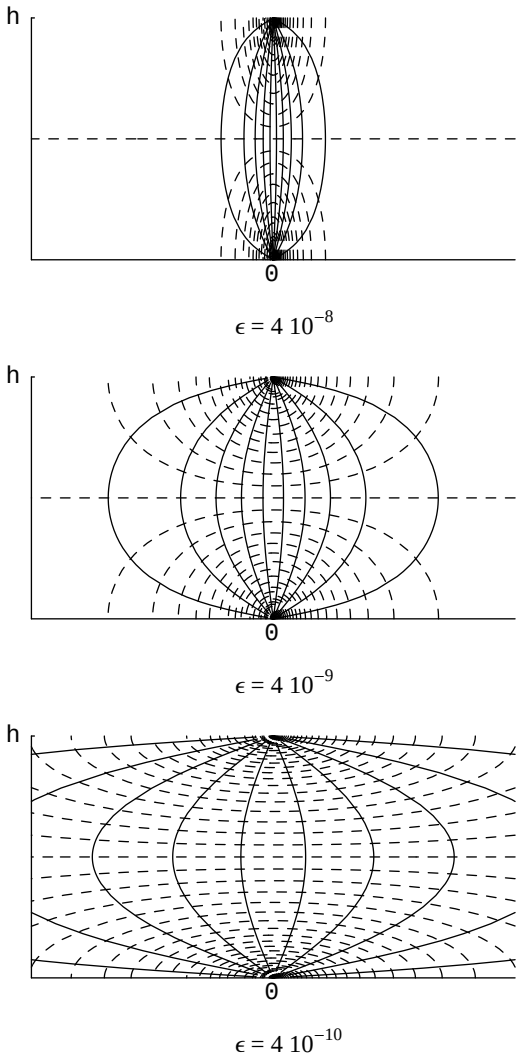

Fig. 5. Shape of the current lines in semi-infinite CPP mode for different values of the ratio $\epsilon = \frac{\sigma_y}{\sigma_x}$. There is a constant current step between two successive lines. The current source and sink are the points of coordinates (0,h) and (0,0) respectively.

the inter-electrode spacing, since by varying this spacing, the ratio of the resistances $\frac{R_{\mathrm{CIP}}}{R_{\mathrm{CPP}}}$ is varied. It is worthy to notice that because of the point-like electrodes, the resistance measured between the two electrodes should diverge. In order to avoid this phenomenon, the extension of the electrodes must be taken into account (see Appendix A.1).

2.2 Rectangular sample

The previous calculation, yielding simple equations, is only valid for macroscopic samples (because of the assumption of an infinite length). To model microscopic systems, we must consider the case of a rectangular sample (see Fig. 17, rectangle 2). In order to avoid the divergence of the resistance, we take into account the finite size of the electrodes. As previously, we use the conformal transformations to determine the shape of the current lines in the system. The result is shown in Figure 8 for the CPP configuration.

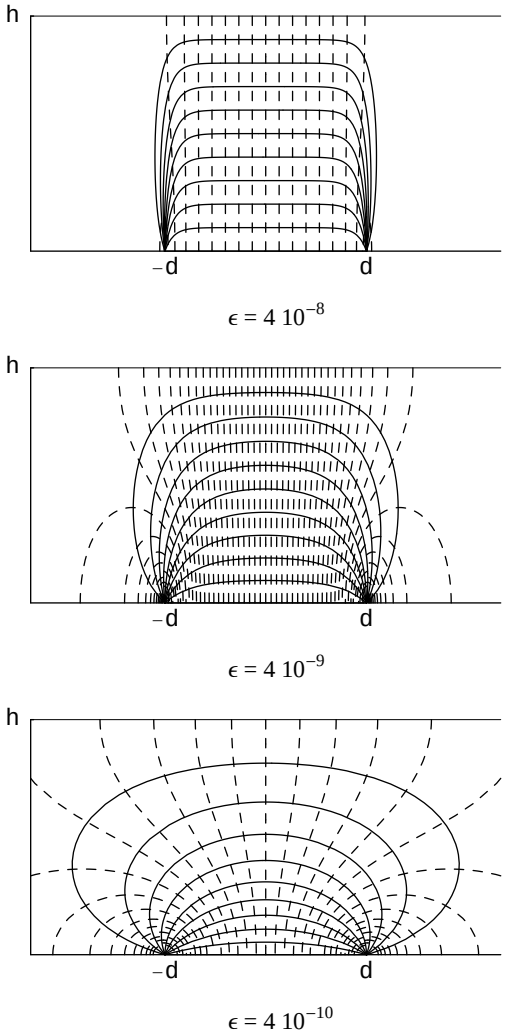

Fig. 6. Shape of the current lines in CIP mode with finite thickness for different values of the ratio $\epsilon = \frac{\sigma_y}{\sigma_x}$. There is a constant current step between two successive lines. The current source and sink are the points of coordinates $(-d,0)$ and $(d,0)$ respectively. The dashed lines represent the equipotentials.

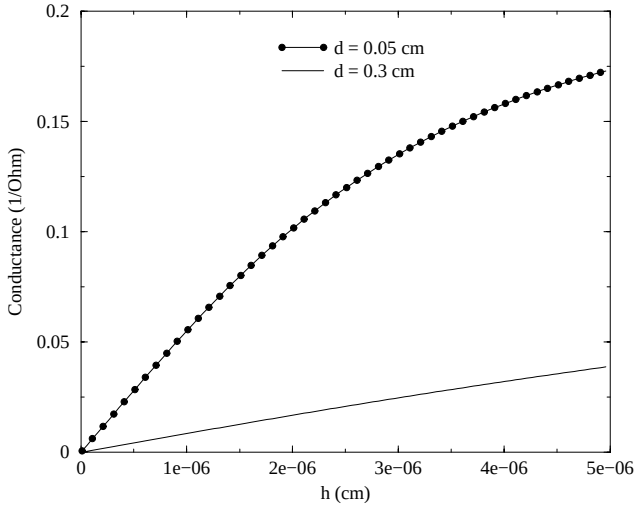

Fig. 7. CIP Conductance of a multilayer as a function of the thickness d for different values of the distance between two electrodes. The non-linearity of the resistance is shown by the curve with $a = 0.05$ cm.

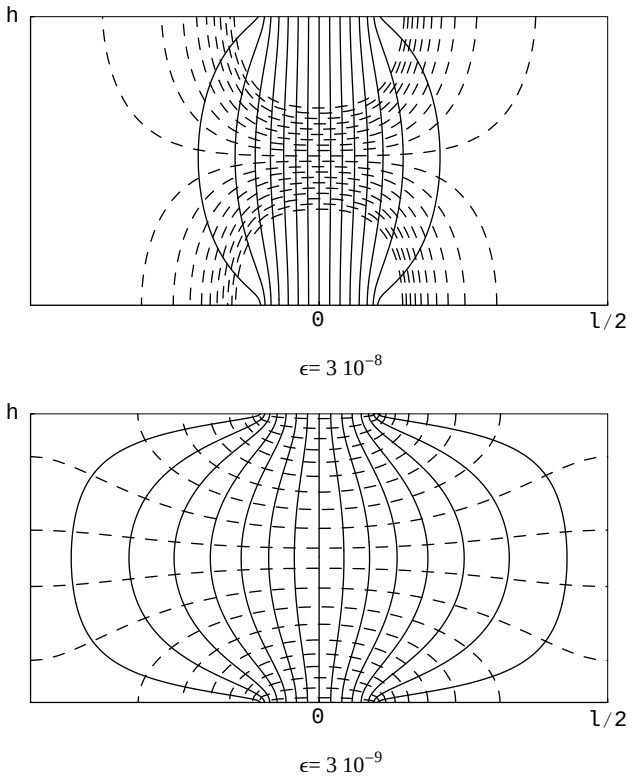

Fig. 8. Shape of the current lines in CPP mode for a sample of limited extension with finite size electrodes and for different values of the ratio $\epsilon = \frac{\sigma_y}{\sigma_x}$. In this example: $\frac{l}{\delta} = 5$. The dashed lines represent the equipotentials.

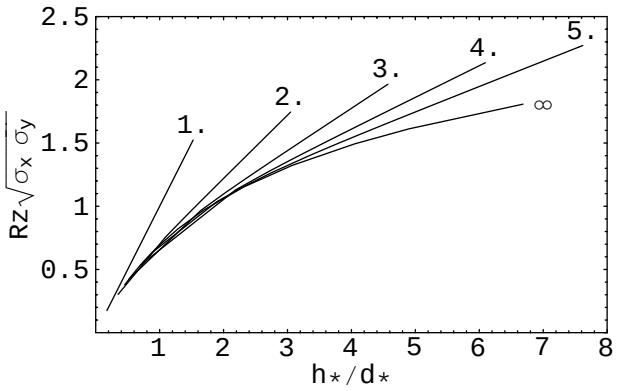

Fig. 9. Characteristic resistance curves calculated by the conformal transformation method in CPP configuration. The resistance is plotted as a function of the reduced parameter $\frac{h^*}{\delta^*}$. Each curve corresponds to a given value of $\frac{l^*}{\delta^*}$.

As in the semi-infinite case (see Fig. 5), it appears that the shape of the current lines strongly depends on the ratio $\epsilon = \frac{\sigma_y}{\sigma_y}$. The resistance of such a sample is shown in Figure 9 as a function of the reduced parameter $\frac{h^*}{\delta^*}$ with $h^* = \frac{h}{\sqrt{\sigma_y}}$ and $\delta^* = \frac{\delta}{\sqrt{\sigma_x}}$ where h is the height of the rectangle, and δ the width of the electrodes. Because of the calculation method (see Appendix A.2), and in order to keep a more general expression, the y-axis does not

straightly represent the resistance R, but $Rz\sqrt{\sigma_x\sigma_y}$. Such an abacus is available for any system, given its dimensions. One notices that, as expected, the curve for $\frac{l^*}{\delta^*} = 1$ (where l is the length of the sample and $l^* = \frac{l}{\sqrt{\sigma_x}}$) is a straight line the slope of which is 1, *i.e.*: for a system with electrodes as large as the sample, the resistance is proportional to the aspect ratio of the rectangle. If the width of the sample is then increased as compared to the size of the electrodes, then the resistance decreases, becomes non-linear with h^* and reaches a limit represented by the curve $l^* = \infty$ which corresponds to an infinite stripe with finite electrodes.

The continuous approximation allows to derive scaling behaviors for the transport properties in these anisotropic materials. However, it is valid only if the extension of the current lines covers a large number of metallic planes which is not always the case in experiments. In particular if the spacing between metallic layers is large, all of the current may flow only in the first metallic plane. The material in CIP configuration cannot then be treated in an homogeneous approximation.

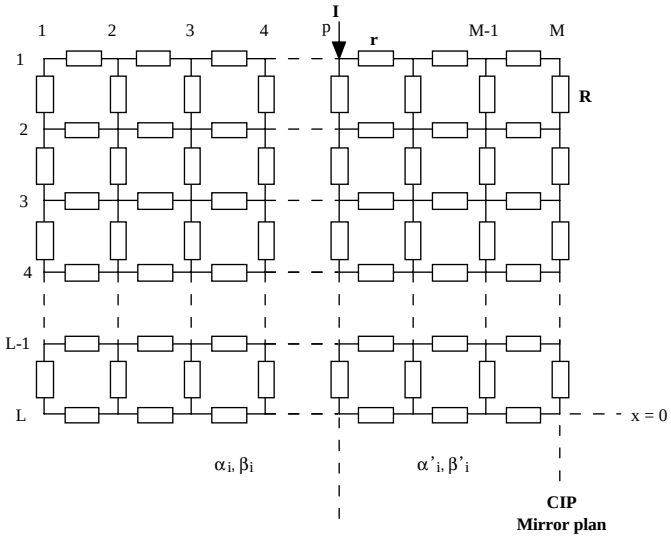

Fig. 10. Model of multilayer using a network of anisotropic resistance. The current source is placed on top of the pth column, and the potential at every intersection is noted V_i^n.

3 Anisotropic network of resistances

In order to get a better description of the transport properties of the multilayers in CIP transport when $R_{\mathrm{CIP}} \gg R_{\mathrm{CPP}}$ or when the number of planes is small, we now take into account the discreetness of the system by considering it as a network of resistances consisting of L lines (*i.e.*, L metallic layers) and M clusters in each line. This network is a 2D system, so that the system is considered invariant by translation along the z-axis. Two different values of resistance are introduced in order to simulate the anisotropy of the multilayer:

- r is the in-plane resistance corresponding to the resistance of a tunnel junction separating two neighbouring clusters within the same plane;
- R is the out-of-plane resistance corresponding to the resistance of the tunnel junction between two clusters of successive planes;
- $q = \frac{r}{R}$.

It should be noticed that the small number of planes in the growth direction (usually about ten) is better described by this method. Furthermore, this technique may be used to study inhomogeneous multilayers in which the resistance between two successive planes may vary from one plane to another (various oxide thickness for instance). We point out that in reference [10], a discreetness was also introduced in the direction perpendicular to the plane but the layers themselves were treated as continuous. This approximation is reasonable for macroscopic samples but may also reach a limit for microscopic samples prepared by lithography because of the reduced number of clusters in each layer (in this case, typically 100×100 for a $1\ \mu\mathrm{m} \times 1\ \mu\mathrm{m}$ junction).

3.1 Simulation of a CIP measurement

We first describe the technique in the CIP configuration. We are interested in the value of the potentials at every intersection of the network. This potential is noted V_i^n where i represents the lines and n the columns (see Fig. 10).

Using the Kirschoff law at the intersections: $\sum I = 0$, and the Ohm law, the following relations are obtained:

$$\begin{cases} i \neq 1, L\text{:}\ \ V_i^{n+1} = 2(1+q)V_i^n - qV_{i-1}^n - V_i^{n-1} - qV_{i+1}^n \\ i = 1, L\text{:}\ \ V_i^{n+1} = 2\left(1+\frac{q}{2}\right)V_i^n - qV_{i-1}^n - V_i^{n-1}. \end{cases}$$

The first and last lines of the sample have to be distinguished from the others, since they have only one neighbouring plane instead of two.

So, the system may be represented by the iterative equation:

$$V^{n+1} = AV^n - V^{n-1}$$

where A is the $(L \times M)$ matrix:

$$\begin{pmatrix} 2+q & -q & 0 & 0 & 0 \\ -q & 2(1+q) & -q & 0 & 0 \\ 0 & -q & \ddots & -q & 0 \\ 0 & 0 & -q & 2(1+q) & -q \\ 0 & 0 & 0 & -q & 2+q \end{pmatrix}.$$

This matrix is then diagonalized, and the potentials in the multilayer are represented by a matrix U with $U = P^{-1}V$ (where P is the matrix that diagonalizes A, and V the matrix of the potentials in the physical system):

$$U_i^n = \alpha_i \mu_i^n + \beta_i \eta_i^n \tag{1}$$

where α_i and β_i are coefficients determined by the boundary conditions which will be determined further and η_i

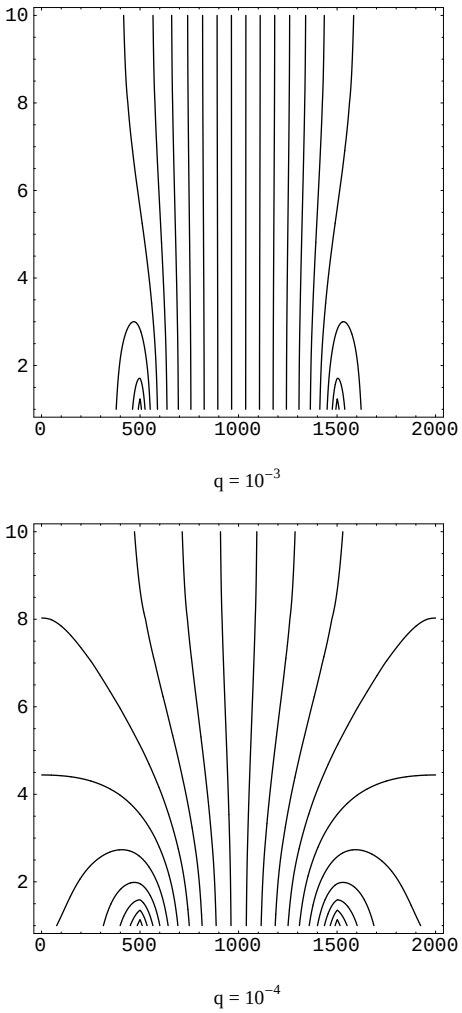

Fig. 11. Map of the equipotential lines obtained for different values of q using a network of resistance and 10 layers in CIP mode. There is a constant potential step ΔV between two successive lines.

and μ_i are the eigenvalues of the matrix A. It is important to notice that the first eigenvalue of A is 2. Therefore, the first line of the multilayer is represented by an arithmetic series: $U_1^n = \alpha_1 n + \beta_1$.

In order to make the calculation easier, we use a vertical plane as symmetry plane. This symmetry plane can be considered connected to the ground (first condition). Furthermore, we assume that no current flows perpendicular to the left side of the sample (second condition), the boundary conditions are written:

$$\begin{cases} 1) & V^M = 0 \\ 2) & V^{-1} - V^0 = 0. \end{cases}$$

Finally, by calculating the coefficients α_i and β_i (see Appendix B.1), U is known everywhere, and the matrix of potentials in "real" space V may be determined by the equation: $V = PU$. It is therefore possible to plot a map of the potentials (see Fig. 11). One notices that in this model, even in the case of a strong anisotropy, the current is forced to flow through at least one metallic layer.

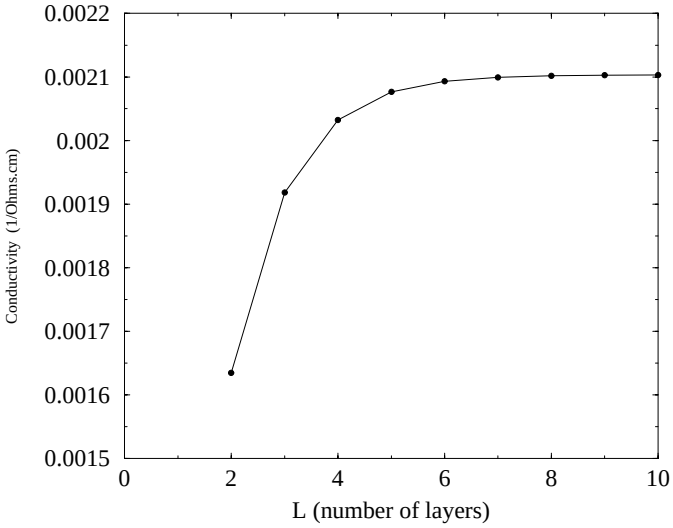

Fig. 12. Resistance in CIP mode as a function of the number of layers L for $q = 10^{-5}$ and $r = 1\ \Omega$.

The resistance is given by:

$$R_{\mathrm{CIP}} = 2\left|\frac{\sum_{i=1}^{L} \Psi_i^{(1)} U_i^p}{I}\right| = 2\frac{V_1^p}{I} \qquad (2)$$

where $\Psi_i^{(n)}$ is the first component of the ith eigenvector. Figure 12 shows the conductivity plotted versus the number of layers. It exhibits a non-linear behavior, and in this example, it appears that the most important part of the current flows in the ten first layers.

3.2 Simulation of a CPP measurement

In CPP mode, the general technique is the same, but the boundary conditions are modified: the plane $x = 0$ is now taken to be a mirror plane.

The boundary conditions are then written

$$\begin{cases} 1) & V^1 - V^0 = 0 \\ 2) & V^M - V^{M-1} = 0 \\ 3) & V_L^n = 0\ \forall n \end{cases}$$

where the two first conditions express that no current flows respectively through the left and right sides of the sample and the third one expresses that the Lth plane is grounded (see the details of the calculation in Appendix B.2).

Figure 13 shows a map of equipotential lines. The resistance is still given by formula 2 because of the symmetry consideration (see Fig. 14): thanks to the chosen symmetry planes, the expression of the resistance is always twice the potential of the electrode. Once more, Figure 14 clearly shows the non-linearity of the CPP resistance versus spacing of the voltage contacts.

As can be seen in Figures 11 and 13, for large values of M (number of clusters within a given plane), the network behaves as the anisotropic continuous approximation, demonstrating that this approximation is correct in

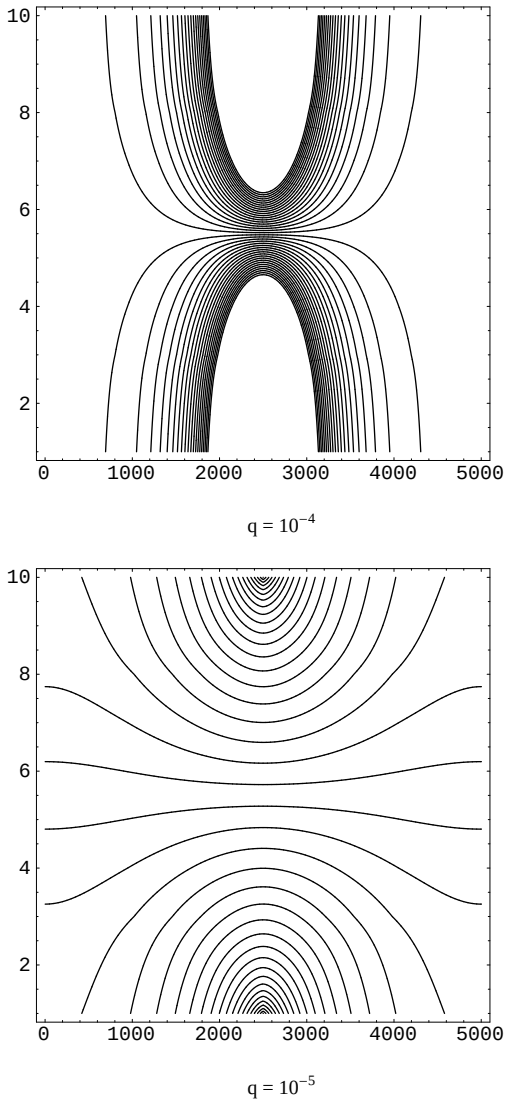

Fig. 13. Map of the equipotential lines obtained for different values of q and $L = 10$, using a network of resistance in CPP mode.

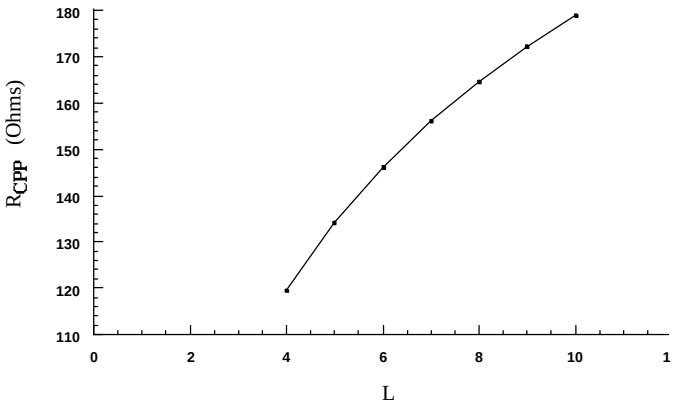

Fig. 14. Resistance in the CPP mode as a function of L for $q = 10^{-5}$ and $r = 1\ \Omega$.

this limit. Moreover, the resistance variations versus distance between contacts for discrete and continuous models both indicate differences from the classic law: $R = \frac{\rho l}{S}$ due to the combined effect of CIP and CPP transport in these systems.

4 Conclusion

In this paper, we presented 2 methods to determine the shape of the current lines in discontinuous multilayers and calculate the CIP and CPP resistances. The comparison of the results obtained by the network of resistances and those obtained in a continuous anisotropic system showed that this last approximation is correct in the limit where the current lines extend over a large number of metallic planes.

These calculations also demonstrated that when R_{CIP} and R_{CPP} are of the same order of magnitude, the measured transport properties are a combination of both CIP and CPP transport making difficult the interpretation of the experimental I(V) curves. Furthermore, the active area through which the current flows in a CPP measurement strongly depends on the ratio $\frac{\sigma_y}{\sigma_x}$, changing from the electrode surface to the surface of the whole sample. Similarly, in CIP mode, the number of layers in which a non-negligible current flows depends on this ratio. It is therefore necessary to be very cautious when interpreting I(V) curves for such samples which cannot correctly be modeled by the Simmons equation [11].

The authors wish to thank Pascale Bayle-Guillemaud for the TEM pictures of Figure 2.

Appendix A: Details of the conformal transformation technique

In this calculation, we consider the discontinuous multilayers as continuous samples with anisotropic conductivity: (σ_x, σ_y) due to the different spacings between clusters in and out of plane. In order to determine the shape of the current lines and the resistance of the samples, we use complex variables and conformal transformations. This technique only allows 2D calculations in the (x, y) plane. Therefore, the electrodes are supposed to be elongated stripes in the z-direction. We then have to solve the equation:

$$\sigma_x \frac{\partial^2 \Phi}{\partial x^2} + \sigma_y \frac{\partial^2 \Phi}{\partial y^2} = 0.$$

Because of the anisotropy of the conductivity, this equation is not a real Laplace equation and then the real and

imaginary parts of Φ do not respect the Cauchy conditions, and the conformal transformations may not be used.

$$\frac{\partial^2 \Phi}{\partial X^2} + \frac{\partial^2 \Phi}{\partial Y^2} = 0$$

so, we need to introduce new variables (X, Y) in the equation describing the system in order to get a Laplace equation (as written above). These new variables are given by:

$$X \to \frac{x}{\sqrt{\sigma_x}},\ Y \to \frac{y}{\sqrt{\sigma_y}}$$

and so on for every length involved in the calculation. This gives rise to an intermediate isotropic system with a conductivity: σ^*. Therefore, the real and imaginary parts of the complex potential $\Phi = \phi + \mathrm{i}\psi$ respect the Cauchy conditions in the (X, Y) plane. Its real part ϕ corresponds to the potential while the imaginary part ψ corresponds to the current.

A.1 Semi-infinite sample

The shape of the current lines in such a system may not be straightly derived because of the boundary conditions expressing that no current flows through the surface of the sample. However, their shape may be derived in a simpler system which is then transformed into an infinite stripe thanks to a conformal transformation. Such a transformation is defined to conserve the angle between two curves so that the orthogonality between the equipotential and the current lines is then conserved[2].

The equation of the current lines is first determined in the simplest system: *i.e.*, the upper semi-plane (ζ, η) (see Fig. 15) in which a source and a sink are placed on the real axis at coordinates $(\pm\ 1)$ (see Fig. 16):

$$V = \frac{a}{\pi} \log \frac{\xi - b}{\xi + b}$$

where π normalizes the current to unity. The transformation leading from the upper semi-plane to an infinite stripe is:

$$Z = \frac{a}{\pi} \log \frac{\xi}{b} \cdot \tag{3}$$

For simplicity, we choose $b = 1$ and a is chosen in order to represent the height of the physical thickness. We immediately find: $a = \frac{h}{\sqrt{\sigma_y}}$ where a corresponds to the height of the rectangle in the (X, Y) plane. So, by replacing ξ by its expression (given by Eq. (3)) in the equation of the complex potential V, we find the equation of the complex potential in the (X, Y) plane, and therefore in the (x, y) plane:

$$\Phi = \log \left\{ \tanh \left[\frac{\pi \sqrt{\sigma_y}}{2h} \left(\frac{x}{\sqrt{\sigma_x}} + \mathrm{i} \frac{y}{\sqrt{\sigma_y}} \right) \right] \right\} \cdot$$

[2] The current and equipotential lines are mutually perpendicular only if the system is isotropic.

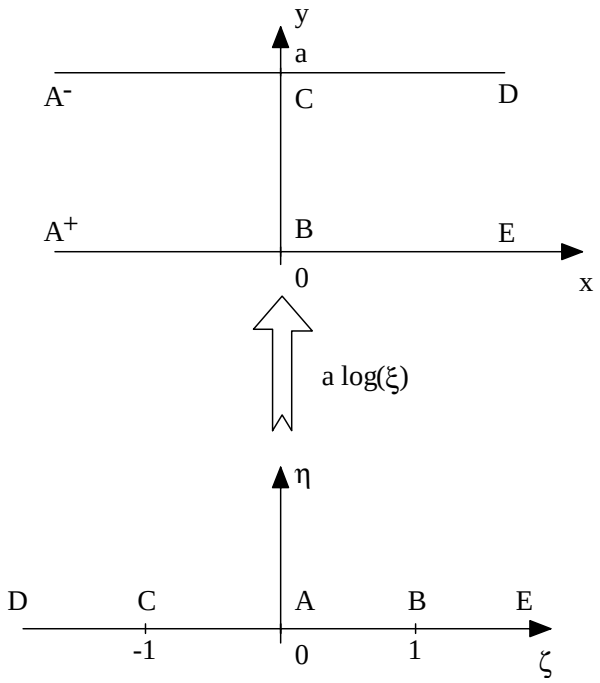

Fig. 15. The two steps of the conformal transformation in the case of an infinite stripe are shown here. In the case of a CPP propagation, the electrodes are placed at the points C and B. In the CIP case, their position are given by $\mathrm{e}^{-\frac{\pi d}{a}}$ and $\mathrm{e}^{\frac{\pi d}{a}}$.

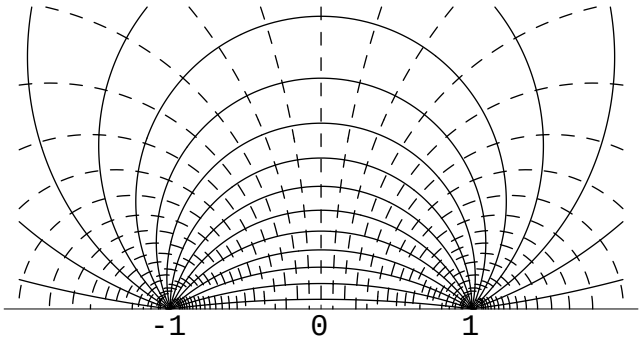

Fig. 16. Equipotentials (top) and current lines (bottom) in the upper semi-plane. The dashed lines represent the equipotential lines.

The shape of the current lines (imaginary part ψ of Φ) is shown in Figure 5 for different values of the ratio $\epsilon = \frac{\sigma_x}{\sigma_y}$.

To calculate the resistance of the sample, we consider the expression of the real part of Φ:

$$\phi = \frac{1}{2} \log \left[\frac{\cosh \frac{\pi x}{h} \sqrt{\frac{\sigma_y}{\sigma_x}} - \cos \frac{\pi y}{h}}{\cosh \frac{\pi x}{h} \sqrt{\frac{\sigma_y}{\sigma_x}} + \cos \frac{\pi y}{h}} \right] \cdot$$

In order to avoid the divergence of the potential on the electrodes, we give these electrodes a finite size Δ, and we assume that the interface between the sample and these electrodes has the same shape as the equipotential lines

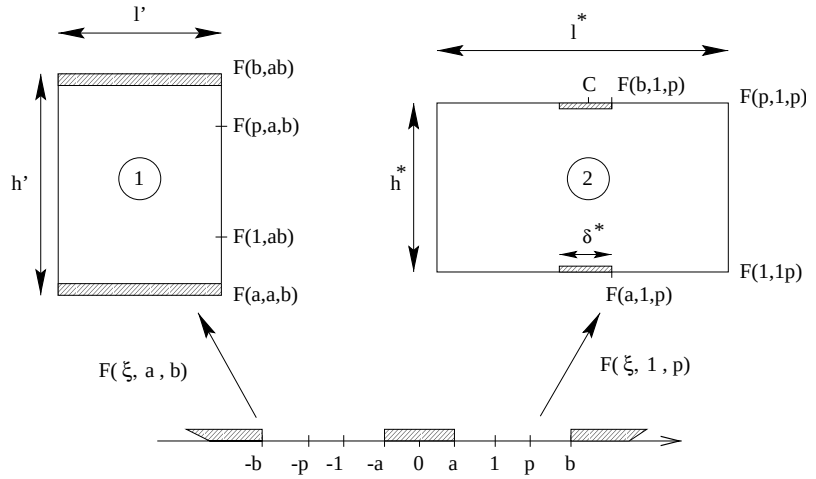

Fig. 17. Description of the different steps of the transformation: the resistance of the system is simply proportional to the aspect ratio of the rectangle 1, the rectangle 2 being the physical one after renormalization by the square root of the conductivities. In the upper semi-plane (ζ,η), one of the electrodes extends from $-a$ to $+a$ while the other extends from $+b$ to $+\infty$ and from $-b$ to $-\infty$, since the points ($\pm\infty$) become a single point after transformation (corresponding to the point C).

calculated above. Within this assumption, the presence of the electrodes does not perturb the system.

The resistance is then simply given by:

$$R_{CPP} = \frac{1}{I}\left[\Phi_{\substack{x=\Delta\\y=0}} - \Phi_{\substack{x=\Delta\\y=h}}\right].$$

This yields:

$$R_{\mathrm{CPP}} = \frac{1}{\pi}\log\left|\frac{\cosh\left(\frac{\pi\Delta}{h}\sqrt{\frac{\sigma_y}{\sigma_x}}\right)+1}{\cosh\left(\frac{\pi\Delta}{h}\sqrt{\frac{\sigma_y}{\sigma_x}}\right)-1}\right|.$$

In CIP mode, the transformation used is the same as in CPP mode. The only difference is the position of the electrodes. In order to obtain two electrodes on the same side, we have to place the corresponding points in the semi-plane on the positive side of the ζ-axis, on both sides of the point $+1$ which will become the origin of the (x, y) plane after the transformation. If the electrodes in the physical system are placed at the points $+d$ and $-d$, then (according to Eq. (3)) their positions in the semi-plane are:

$$\zeta_1 = \mathrm{e}^{-\frac{\pi d}{a}}$$
$$\zeta_2 = \mathrm{e}^{\frac{\pi d}{a}}.$$

The complex potential is then written:

$$\Phi = \log\left[\frac{\mathrm{e}^{\frac{\pi\sqrt{\sigma_y}}{h}\left(\frac{x}{\sqrt{\sigma_x}}+\mathrm{i}\frac{y}{\sqrt{\sigma_y}}\right)} - \mathrm{e}^{-\frac{\pi d}{h}\sqrt{\frac{\sigma_y}{\sigma_x}}}}{\mathrm{e}^{\frac{\pi\sqrt{\sigma_y}}{h}\left(\frac{x}{\sqrt{\sigma_x}}+\mathrm{i}\frac{y}{\sqrt{\sigma_y}}\right)} - \mathrm{e}^{\frac{\pi d}{h}\sqrt{\frac{\sigma_y}{\sigma_x}}}}\right]$$

and the shape of the corresponding current lines is shown in Figure 6.

The real part (corresponding to the potential) is given by:

$$\phi = \log\left[\mathrm{e}^{-\frac{2\pi d}{h}\sqrt{\frac{\sigma_y}{\sigma_x}}}\left(\frac{\cosh\frac{\pi(d+x)}{a}\sqrt{\frac{\sigma_y}{\sigma_x}} - \cos\frac{\pi y}{h}}{\cosh\frac{\pi(d-x)}{a}\sqrt{\frac{\sigma_y}{\sigma_x}} - \cos\frac{\pi y}{h}}\right)\right]$$

which yields an expression of the resistance:

$$R_{\mathrm{CIP}} = \log\left[\frac{\cosh\frac{2\pi d}{h}\sqrt{\frac{\sigma_y}{\sigma_x}}-1}{\cosh\frac{\pi\Delta}{h}\sqrt{\frac{\sigma_y}{\sigma_x}}-1}\right]$$

where Δ is the width of the electrodes.

A.2 Rectangular sample

As in the case of a semi-infinite sample, the shape of the current lines in such a system cannot be straightly calculated. However, if we consider a rectangle the two opposite sides of which are equipotentials, the current lines and the equipotentials are simply the vertical and horizontal lines respectively (Fig. 17, rectangle 1). So, we have to find a transformation that transforms this rectangle into the physical system (see Fig. 17, rectangle 2). This is made by the well-known Schwarz-Cristoffel transformation which transforms the upper semi-plane into a closed polygon, assuming an intermediate step: the upper semi-plane, as shown in Figure 17. This kind of calculations has already been performed in the case of an isotropic rectangle with punctual electrodes [12] in order to determine the conversion factors leading to the resistance by square. However, in our case, the simulation is made with finite electrodes. We write here the Schwarz-Cristoffel transformation for a rectangle, and its inverse function (which is a function of the Jacobi Elliptic function).

The Schwarz-Cristoffel transformation is given by:

$$Z = A\int_0^{\xi} \frac{\mathrm{d}t}{\sqrt{(t^2-\alpha^2)\,(t^2-\beta^2)}} + B = AF(\xi,\alpha,\beta) + B$$

where the points $(\pm\alpha)$, $(\pm\beta)$ (called characteristic points) in the upper semi-plane (ζ,η) correspond to the angles of the rectangle in the Z plane, and $B = 0$ if $\xi = 0$ corresponds to $z = 0$.

Its Inverse function is defined as:

$$\xi = \frac{1}{\alpha}\mathrm{Sn}\left(\beta Z,\, \frac{\alpha^2}{\beta^2}\right).$$

Knowing h, l (respectively the height and length of the physical system) and δ the width of the electrodes, we have to deduce 4 important points in the upper semi-plane (instead of 2 for the infinite stripe): two of them (a and b) corresponding to the width of the electrodes, while the two others (p and q) stand for the coordinates of the corners of the rectangle. For simplicity, we choose $q = 1$. So, starting from the upper semi-plane, if we choose $\alpha = 1$ and $\beta = p$, the Schwarz-Cristoffel transformation leads to the physical system. On the opposite, if we choose $\alpha = a$ and $\beta = b$, it leads to a rectangle the two horizontal sides of which are the electrodes. As in the case of a semi-infinite sample, every length involved in the calculation is redimensioned (and called equivalent length) and denoted by a star: $l^* = \frac{l}{\sqrt{\sigma_x}}$ and $h^* = \frac{h}{\sqrt{\sigma_y}}$. The values of the points p, a and b are now simply deduced from geometrical considerations. In order to calculate the value of p, the following equation has to be solved (which is done in a numerical way):

$$\mathrm{Arg}[F(p,1,p)] = -\mathrm{ArcTan}\left(\frac{2h^*}{l^*}\right)$$

where Arg is the function giving the argument of a complex number.

Knowing p, we may deduce the value of the Schwarz-Cristoffel pre-factor A:

$$A = \frac{2F(1,1,p)}{l^*}.$$

Finally, a and b corresponding to the position of the electrodes are deduced: a is given by:

$$F(a,1,p) = A\frac{\delta^*}{2}$$

and b may be deduced:

$$F(a,1,p) = \mathrm{Re}[F(b,1,p)].$$

So, by now applying the Schwarz-Cristoffel $F(\xi,a,b)$, we obtain the rectangle 1. Its two opposite sides are equipotentials, and its aspect ratio is proportional to the resistance of the physical rectangle. This aspect ratio is given by:

$$R' = \frac{1}{2}\tan[\mathrm{Arg}[F(b,b,a)]].$$

In order to determine the expression of the resistance of the real system, we may write the current flowing through the system:

$$I = jS = \frac{\sigma^* z\delta' V}{h'}$$

where $\frac{V}{h'}$ is the electric field, z: the depth of the system, σ^* the conductivity, δ' and h' respectively the width and height of rectangle 1. The resistance is then simply given by:

$$R = \frac{h'}{\sigma^* z\delta'}$$

$\frac{h'}{\delta'}$ being the aspect ratio of rectangle 1, we may write:

$$R' = R\sigma^* z.$$

To determine the expression of σ^*, we compare the expression of the resistance of a rectangle the electrodes of which occupy the whole width of the sample, before and after the normalization of the distances:

- Before renormalization: $R = \frac{h}{\sigma^* z\delta}\sqrt{\frac{\sigma_x}{\sigma_y}}$
- After renormalization: $R = \frac{h}{\sigma_y z\delta}$.

By identification, we obtain:

$$\sigma^* = \sqrt{\sigma_x\sigma_y}.$$

This yields the relation between R and R':

$$R' = Rz\sqrt{\sigma_x\sigma_y}$$

which is the vertical axis of Figure 9.

Finally, knowing the shape of the current and equipotential lines in such a simple system (they are vertical and horizontal lines, respectively), we may apply the reverse process to obtain their equations in the physical system:

- In rectangle 1:

$$\Phi' = \mathrm{i}\frac{V_1 - V_2}{2}\frac{z}{h'} + \frac{V_1 + V_2}{2}$$

  where V_1 and V_2 are the potentials of the electrodes.
- In rectangle 2 (after applying the successive conformal transformations):

$$\Phi = \mathrm{i}\frac{V_1 - V_2}{2h}F\left(F^{-1}\left(\frac{x}{\sqrt{\sigma_x}} + \mathrm{i}\frac{y}{\sqrt{\sigma_y}}, 1, p\right), a, b\right) + \frac{V_1 + V_2}{2}.$$

The calculations for the CIP mode are not detailed here, since the results may be obtained by the same process and by changing the positions of the characteristic points of the Schwarz-Cristoffel transformation.

Appendix B: Details of the calculation in the case of a network of resistances

The multilayer is now represented by a network of resistances in which we are interested by the value of the potentials at each intersection (see Fig. 10). The system is mathematically represented by a matrix V.

B.1 CIP configuration

In order to make the calculation easier, we use the symmetry of the system and assume a vertical plane to be a mirror plane (it is therefore equipotential and linked to the ground: *i.e.* $V_{\underset{\text{plane}}{\text{mirror}}} = 0$). This means that the studied system contains $(2M-1)$ clusters in each plane and L metallic layers, but the calculations will be made with only M clusters and a single source (which will become a sink by symmetry).

The characteristic equation $X^2 - \lambda_i X + 1 = 0$ of the system, corresponding to the series $V^{n+1} = AV^n - V^{n-1}$ obtained by applying the Kirschoff's law, (where λ_i are the eigenvalues of the matrix A) is easily solved. We find two solutions noted μ_i and η_i:

$$\begin{cases} \mu_i = \frac{\lambda_i - \sqrt{\lambda_i^2 - 4}}{2} \\ \eta_i = \frac{\lambda_i + \sqrt{\lambda_i^2 - 4}}{2}. \end{cases}$$

The system is now described in the eigenvectors space by the equation: $U_i^n = \alpha_i \mu_i^n + \beta_i \eta_i^n$.

To determine the potentials, the system is separated into two parts on both sides of the source, so that we have 8 coefficients to determine: α_1, α_i, β_1, β_i (on the left side of the source), and α'_1, α'_i, β'_1, β'_i (on the right side), since as explained in Section 3.1, the first line has to be distinguished from the others because its corresponding eigenvalue is equal to 2. In order to fully determine the system of equations, it is necessary to introduce the linking condition between these two parts. The source is therefore considered as point-like, and located on top of the pth column. This perturbation is represented by the vector S given by:

$$S = \begin{pmatrix} I \\ 0 \\ \vdots \\ 0 \\ 0 \end{pmatrix}.$$

These boundary conditions give rise to a system of 6 equations which has to be solved:

$$\begin{cases} \alpha_1 + \beta_1 = \beta_1 \\ \alpha_i \eta_i + \beta_i \mu_i - \alpha_i - \beta_i = 0 \\ \alpha'_1 M + \beta'_1 = 0 \\ \alpha'_i \eta_i^M + \beta'_i \mu_i^M = 0 \\ U^p_{1(\text{left})} = U^p_{1(\text{right})} \\ U^p_{i(\text{left})} = U^p_{i(\text{right})}. \end{cases}$$

By combining the 4 first equations, we obtain:

$$\begin{cases} \alpha_1 = 0 \\ \alpha_i = -\beta_i \frac{\mu_i - 1}{\eta_i - 1} \\ \alpha'_1 = -\frac{\beta'_1}{M} \\ \alpha'_i = -\beta'_i \left(\frac{\mu_i}{\eta_i}\right)^M \\ \beta'_1 \left(1 - \frac{p}{M}\right) \\ \beta_i = \beta'_i \frac{1 - \left(\frac{\mu_i}{\eta_i}\right)^{M-p}}{1 - \frac{\mu_i - 1}{\eta_i - 1}\left(\frac{\eta_i}{\mu_i}\right)^p}. \end{cases}$$

Finally, the introduction of the source with a current unity creates a perturbation which is taken into account by applying the Kirschoff's law on the pth column. The result of the Kirschoff's law is then converted to be applied to the matrix U and gives:

$$U^{p+1} + U^{p-1} = (P^{-1}AP)U^p + P^{-1}\begin{pmatrix} 1 \\ 0 \end{pmatrix}$$

where $P^{-1}AP$ is simply the ith eigenvalue λ_i of the matrix A (depending on the number i of the studied line).

This finally yields:

$$\begin{aligned} \beta'_i = -P^{-1}S \Bigg[& \eta_i^{p+1} \left(1 - \left(\frac{\eta_i}{\mu_i}\right)^{M-p-1}\right)\left(1 - \frac{\eta_i - 1}{\mu_i - 1}\left(\frac{\mu_i}{\eta_i}\right)^p\right) \\ & + \left(1 - \left(\frac{\eta_i}{\mu_i}\right)^{M-p}\right)\left(1 - \frac{\eta_i - 1}{\mu_i - 1}\left(\frac{\mu_i}{\eta_i}\right)^{p-1}\right)\eta_i^{p-1} \\ & - \lambda_i \left(\eta_i^p - \left(\frac{\eta_i}{\mu_i}\right)^M \mu_i^p\right)\Bigg]^{-1}; \\ \alpha'_i = -\beta'_i & \left(\eta_i^p - \left(\frac{\eta_i}{\mu_i}\right)^M \mu_i^p\right); \\ \beta_i = \beta'_i & \frac{1 - \left(\frac{\eta_i}{\mu_i}\right)^{M-p}}{1 - \frac{\eta_i - 1}{\mu_i - 1}\left(\frac{\mu_i}{\eta_i}\right)^p}; \\ \alpha_i = -\beta_i & \frac{\eta_i - 1}{\mu_i - 1}; \\ \beta'_1 = -MP^{-1}S; & \\ \alpha'_1 = -\frac{\beta'_1}{M}; & \\ \beta_1 = \beta'_1 & \left(1 - \frac{p}{M}\right); \\ \alpha_1 = 0. & \end{aligned}$$

The matrix U is now completely defined, and we may deduce the value of every element of the matrix V by using the relation: $V = PU$.

B.2 CPP configuration

The boundary conditions are now modified. No current flows through the lateral sides of the sample, and the plane

$x = 0$ is considered as a mirror plane. Since this plane is considered to be a mirror plane, it appears that it is necessary to distinguish the two cases of odd or even number of layers. For example, if the simulation is made with $L = 5$, this means that there are 10 or 11 layers, depending on the matrix which is used, *i.e.* the exact symmetry plane is located either on a metallic plane or between two successive metallic planes.

In the odd case,

$$\begin{pmatrix} 2+q & -q & 0 & 0 & 0 \\ -q & 2(1+q) & -q & 0 & 0 \\ 0 & -q & \ddots & -q & 0 \\ 0 & 0 & -q & 2(1+q) & -q \\ 0 & 0 & 0 & -q & 2(1+q) \end{pmatrix}.$$

In the even case:

$$\begin{pmatrix} 2+q & -q & 0 & 0 & 0 \\ -q & 2(1+q) & -q & 0 & 0 \\ 0 & -q & \ddots & -q & 0 \\ 0 & 0 & -q & 2(1+q) & -q \\ 0 & 0 & 0 & -q & 2+3q \end{pmatrix}.$$

As in the CIP case, the coefficients determining the elements of the matrix U must be calculated thanks to the boundary conditions. It is important to notice that because no eigenvalue is equal to 2, every layers are represented by an equation similar to equation 1, so that there are only 4 coefficients to calculate: $\alpha_i,\ \beta_i,\ \alpha'_i,\ \beta'_i$.

The boundary conditions expressing that no current flows through the left and right side of the sample and that the plane $x = 0$ is grounded and the linking condition lead to the new system of equations:

$$\begin{cases} \alpha_i\eta_i + \beta_i\mu_i - \alpha_i - \beta_i = 0 \\ \alpha'_i\eta_i^M + \beta'_i\mu_i^M - \alpha'_i\eta_i^{M-1} - \beta'_i\mu_i^{M-1} = 0 \\ U^p_{i(\text{left})} = U^p_{i(\text{right})}. \end{cases}$$

By combining these equations and by introducing the linking condition (which has the same expression as in the CIP configuration given by the Eq. (B.1)), we find:

$$\begin{aligned} \beta'_i = -P^{-1}S \Bigg[& \frac{\eta_i^{M-1} - \eta_i^M}{\mu_i^M - \mu_i^{M-1}}\mu_i^{p+1} + \eta_i^{p+1} \\ & + \left(\frac{\frac{\eta_i^{M-1} - \eta_i^M}{\mu_i^M - \mu_i^{M-1}}\mu_i^p + \eta_i^p}{\frac{1-\eta_i}{\mu_i - 1}\mu_i^n + \eta_i^n} \right) \left(\frac{1-\eta_i}{\mu_i - 1}\mu_i^{p-1} + \eta_i^{p-1} \right) \\ & - \lambda_i \left(\frac{\eta_i^{M-1} - \eta_i^M}{\mu_i^M - \mu_i^{M-1}}\mu_i^p + \eta_i^p \right) \Bigg]; \\ \alpha'_i = \beta'_i & \frac{\eta_i^{M-1} - \eta_i^M}{\mu_i^M - \mu_i^{M-1}}; \\ \beta_i = \beta'_i & \frac{\frac{\eta_i^{M-1} - \eta_i^M}{\mu_i^M - \mu_i^{M-1}}\mu_i^p + \eta_i^p}{\frac{1-\eta_i}{\mu_i - 1}\mu_i^p + \eta_i^p}; \\ \alpha_i = \beta_i & \frac{1-\eta_i}{\mu_i - 1}. \end{aligned}$$

References

1. B. Dieny *et al.*, Journ. Magn. Magn. Mater **185**, 283 (1998).
2. S. Sankar, B. Dieny, A. Berkowitz, J. Appl. Phys. **81**, 5512 (1997).
3. N. Julliere, Phys. Lett. A **54**, 225 (1975).
4. J.I. Gittleman, Y. Goldstein, S. Bozowski, Phys. Rev. B **5**, 3609 (1972).
5. P. Sheng, B. Abeles, Y. Arie, Phys. Rev. Lett. **31**, 44 (1973).
6. W.P. Pratt *et al.*, Phys. Rev. Lett. **66**, 3060 (1991).
7. J. Barnas, A. Fert, Phys. Rev. Lett. **80**, 1058 (1998).
8. S. Takahashi, S Maekawa, Phys. Rev. Lett. **80**, 1758 (1998).
9. E. Durand, *Electrostatique, Tome II* (Masson et Cie, 1966), p. 308
10. G.N. Kakazei *et al.*, *Communication DS09 at Intermag 2000, April 9-13, 2000, Toronto*, oral presentation.
11. J.G. Simmons, J. Appl. Phys. **34**, 1793 (1963).
12. M.A. Logan, Bell Syst. Tech. J. 2277 (Dec. 1967).